Experimental Mechanics (2015) 55:1465–1474
DOI 10.1007/s11340-015-0062-9

Estimation of the Elastic Properties of Polymer Plates Using a Structured Light Technique

S.-R. Rojas-Ramirez[1,2] · F.-J. Ornelas-Rodriguez[1] · J.B. Hurtado-Ramos[1] · J.-J. Gonzalez-Barbosa[1] · R. Zitzumbo[3]

Received: 1 December 2014 / Accepted: 21 June 2015 / Published online: 1 July 2015

Abstract An experimental device for determining Young's modulus of polymer plates is presented. Two sets of polymer blends were investigated. First samples were made of ethylene propylene diene (EPDM), high density polyethylene (HDPE), and meleic anhydride grafting on polyethylene (PE-MA) reinforced with glass fiber. The second set of samples was made of low density polyethylene (LDPE) reinforced with nylon fiber. Young's modulus of a circular polymeric plate under biaxial stress was determined by measuring its out-of-plane displacement. This test is also known as bulge test. Values of Young's modulus of the polymer plates were compared to those obtained from standard uniaxial tensile tests. Biaxial stress causes tension in all internal reinforcing fibers of the samples, in contrast tensile tests that cause tension mainly in fibers aligned with the applied force. Out-of-plane displacement was measured applying a laser triangulation setup based on a projected laser line and a CCD camera. A mathematical model for plates under the bulge test was then used in Young's modulus calculations using out-of-plane displacement and plate dimensions. It is proved that the bulge test is more sensitive to reinforcement fiber compared to the standard uniaxial tensile test.

Keywords Polymeric plate · Young's modulus · Laser triangulation · Elasticity · Structured light · Bulge test

Introduction

Reinforced polymers are light weight and durable structural composite materials [1]. To improve the reliability of fiber reinforced polymers their mechanical properties must be determined. A bulge test is proposed for determining Young's modulus and stress–strain curves under biaxial stress condition. We tested two polymer blends which are used in the automotive industry. The first polymer blend was made of ethylene propylene diene terpolymer (EPDM) and high density polyethylene (HDPE) reinforced with short glass fiber. The EPDM/HDPE reinforced blend is used on seals of automotive windows and as insulating material for automotive electric cables. The second polymer blend was made of low density polyethylene (LDPE) with Nylon 6 as a reinforcing fiber. The LDPE/Nylon blend is used to manufacture automotive interior parts. Conventionally, Young's modulus and stress–strain curves are obtained from uniaxial tensile tests [2, 3]. Biaxial stress condition is close to daily use conditions of cable insulation and automotive interiors; therefore, the bulge test is considered to be suitable for measuring Young's modulus and stress–strain curves for these materials.

Young's modulus of polymers is determined mainly by standard uniaxial tension tests, in the form of straight-sided and dumbbell-shaped test specimens [2–4]. Straight-sided specimens with tabbed configurations require careful adhesive selection and special specimen preparation. Certain laminated layups are prone to edge delamination which can affect tensile

Electronic supplementary material The online version of this article (doi:10.1007/s11340-015-0062-9) contains supplementary material, which is available to authorized users.

✉ S.-R. Rojas-Ramirez
srojasr1102@alumno.ipn.mx

[1] Instituto Politécnico Nacional, CICATA Querétaro, Cerro Blanco No. 141, Col. Colinas del Cimatario, Qro., Mexico C.P. 76090

[2] Universidad Aeronáutica en Querétaro, Carretera Estatal Querétaro-Tequisquiapan C.P. 22154, Colón Qro, Mexico 76270

[3] CIATEC, A.C, Omega 201, Fracc, Industrial Delta, León Gto, Mexico C.P. 37545

strength results. Dumbbell-shaped test specimens have stress concentration at the radius [4]. As an alternative, the bulge test is used for determining the mechanical properties under biaxial tension conditions with small bending component [5]. Among the different test methods for Young's modulus determination, the bulge test has become popular for sheet metal [6–9], thin films [10–13], polymers [14–28], and biological materials [29]. In comparison to uniaxial tests, higher strain values can be achieved by bulge tests [7, 16] and the maximum strain obtained in uniaxial tensile test before necking is relatively small [6].

The bulge test has been successfully applied [6, 9, 12, 15–24, 26–29] and differences have been observed in comparison with uniaxial tests. This test is suitable for investigating polymer blends for large biaxial plastic deformation prior to failure [16]. Currently, it has been applied for determining stress–strain curves [9, 16, 29], pressure versus out-of-plane displacement curves [20, 29], Young's modulus [28], changes of plate thickness [23, 29], radius of curvature [29], hyperelastic model parameters [24], strain distribution [22], mechanism of bursting [26], transient surface shapes [19], anisotropy coefficients [6], thermally induced changes [14, 25, 27] and mechanical properties of biological tissues [30]. The results presented by many researchers show good agreement with theoretical values and with other methods of testing, such as biaxial extension and uniaxial tension.

In this paper we present the results for determining Young's modulus using the bulge test. These results were compared with those from uniaxial tests for the same materials. Two sets of samples were prepared. The first set of samples was made of ethylene propylene diene terpolymer (EPDM), high density polyethylene (HDPE), and meleic anhydride grafting on PE (PE-MA) reinforced with short glass fiber. The short glass fiber proportions in the polymer blends were 0, 2.2 and 6.9 % given in gravimetric proportion. The second set of samples was made of low density polyethylene (LDPE) with Nylon 6 as a reinforcing fiber. The Nylon 6 fiber proportions in the polymer blends were 0 and 20 % given in gravimetric proportion. Laminated samples about 1.5 mm thick were prepared for the bulge tests. The laminated samples were mounted on an air pressure chamber. Air pressure was applied to a sample of 80 mm in diameter.

For this research a laser triangulation technique was implemented to measure the out-of-plane displacement of a sample plate. The accuracy of laser triangulation systems has been previously reported to be between 10 and 15 μm [31, 32]. This system consisted of a CCD camera with focus lenses and a laser line diode. The laser line is projected to the target and the diffuse reflection of the target is collected by the camera's focus lenses. The projected laser, that is, the reflected laser light to the camera and the imaginary line between the camera and the laser diode form a triangle. The camera's lenses focus an image of the reflected laser line on the sensor array of the camera. The position of the reflected laser line, into the image, changes with the distance to the target. This system was calibrated by the methodology proposed by Bouguet using the camera calibration toolbox [33, 34] from Matlab and was scaled using a reference standard calibration block as a reference for height [35].

Some applied measuring methods for out-of plane displacement in the bulge test are photogrammetry [9, 17, 18], digital image correlation [10, 16, 14, 21], interferometry [12], laser triangulation [19], fringe projection [11, 20], and stereo vision [24]. The most accurate measuring method is interferometry since the resolution is, at least, half of the laser wavelength. Photogrammetry commercial systems are frequently used in bulge test, of which manufacturers declare a strain resolution of 0.005. Fringe projection techniques that use phase-shifting methods for fringe analysis provide high resolution, however it requires multiple images which restricts their scope of applicability to static objects [36]. Spatial fringe analysis methods allow the technique to be applicable for real-time 3D measurements but at the cost of resolution [36]. In the present paper it is desirable to measure the out-of-plane displacement as quickly as possible in order to reduce viscoelastic effects. Using the selected triangulation technique 3.3 frames/s can be analyzed and, as a result, the out-of plane displacement is obtained from a whole diametrical line where the laser impinges. Full field measurement is not essential since reinforcement fiber is randomly oriented and anisotropy is not expected.

The stiffness of reinforced polymer blends has been investigated under uniaxial tension and biaxial stress conditions by the bulge test. Glass fiber increases the stiffness of EPDM/HDPE polymer blends. EPDM/HDPE samples with 0 and 2.2 % have nonsignificant differences on uniaxial Young's modulus. Biaxial Young's modulus is more sensitive to glass fiber content than uniaxial Young's modulus. Nylon fiber increases the stiffness but embrittle the LDPE. Manufacturing and handling of reinforced LDPE samples is difficult, which causes the increment of standard deviation of uniaxial Young's modulus. Uniaxial and biaxial tests have good agreement in the range tested for LDPE samples.

Materials and Methods

Two types of polymer blends were prepared. The first polymer blend was made of ethylene propylene diene terpolymer (EPDM), high density polyethylene (HDPE), and

meleic anhydride grafting on PE (PE-MA) reinforced with short glass fiber. The second polymer blend was made of low density polyethylene (LDPE) with Nylon 6 as a reinforcing fiber.

Preparation of Sample Plates Reinforced With Glass Fiber

The components of the sample plates reinforced with glass fiber were: EPDM supplied by Dow Chemical Company under the trade name Nordel IP 4725P with 70 % of ethylene and 5 % of ethilidene norbornene, HDPE supplied by PEMEX under the trade brand PADMEX 56035, and PE-MA supplied by DuPont under the trade brand fusabond EMB-265D. All of these materials were used as supplied. The polymer plates were reinforced with glass fiber. Glass fiber, with 25 μm in diameter, was crushed in a blade mill equipped with a 1 mm mesh. The glass fiber was mixed with EPDM, HDPE and PE-MA in the proportions specified in Table 1. The polymer blend was extruded to make pellets about 4 cm in length and 3 cm in diameter. The pellets were then crushed in a mill with a 3 mm mesh. The crushed pellets were melted and injected in a mold to make squared plates of 15 cm along a side and about 1.5 mm thick. PE-MA eases incorporation of reinforcement fiber to the blend and increases energy requirements for manufacturing.

Preparation of Sample Plates Reinforced With Nylon

The components of the sample plates reinforced with nylon were LDPE and nylon 6. LDPE is the soft matrix and nylon 6 is the rigid part. Nylon pellets were dried at 80 °C during 4 h. LDPE and nylon 6 were mixed, extruded and pelletized. Pellets were used to make laminated plates of 15 cm along a side and about 1.5 mm thick. Table 2 shows the composition of the nylon reinforced samples.

Biaxial Load Application and Measurement of Out-of-Plane Displacement

Pressurized air was applied to a pressure chamber by means of a proportional pneumatic regulator Festo MPPE-3-1/4-10-0108 which supplied a pressure of 100 kPa/V. The pneumatic regulator provides a constant pressure with a standard deviation about 200 Pa, manufacturer declares a maximum hysteresis of 5 kPa. A direct current voltage was applied to the pneumatic regulator with DC power supply Sorensen XDL 35-5P. The pressure of the chamber was measured with a Festo transducer SDE-10-10 V/20 mA. The voltage output of the transducer was measured and recorded with a NI USB 6008 data acquisition board. The sample plate was fastened with a metal ring with 80 mm inner diameter. Figure 1 shows a scheme of the experimental setup.

Table 1 Composition of glass fiber reinforced samples

Sample	EPDM (%)[a]	HDPE (%)[a]	PE-MA (%)[a]	Glass fiber (%)[a]
1	76.9	23.1	0.0	0.0
2	69.0	20.7	3.4	6.9
3	72.5	21.7	3.6	2.2

[a] Gravimetric proportion

A laser triangulation system was used to measure the out-of-plane displacement of the plate. The measurement system consisted of a CCD camera Marlin F145 with a focus lens array of 8 mm / F 1.4 and a Lasiris SNF laser line generator. The camera Marlin F145 has a CCD with 1392×1040 pixels in resolution. The Lasiris SNF laser emits red light line at 660 nm with 1 mW power, see Fig. 2.

The camera was calibrated using the Bouguet's camera calibration toolbox for Matlab [33] with a 5 mm square grid board. After calibration, the extrinsic parameters A and the intrinsic parameters I_c were obtained. The transformation from the real world to image is the transformation matrix M, see equation (1).

$$M = I_C A = \begin{bmatrix} \frac{f}{h_x} & 0 & u_o \\ 0 & \frac{f}{h_y} & v_o \\ 0 & 0 & 1 \end{bmatrix} \begin{bmatrix} r_{11} & r_{12} & r_{13} & t_x \\ r_{21} & r_{22} & r_{23} & t_y \\ r_{31} & r_{32} & r_{33} & t_z \end{bmatrix} = \begin{bmatrix} m_{11} & m_{12} & m_{13} & m_{14} \\ m_{21} & m_{22} & m_{23} & m_{24} \\ m_{31} & m_{32} & m_{33} & m_{34} \end{bmatrix} \quad (1)$$

where matrix I_C defines the focal length f and the principal point (u_o,v_o), which is the intersection of the principal axis with the image plane. The variables h_x and h_y are the dimensions of the camera's pixels [37]. The elements $I_c(1,1)$ and $I_c(2,2)$ are the focal length expressed in pixels. The matrix A defines the relative position of the reference system in the focal point relative to the reference system in the world, by means of a rotation and a translation, see Fig. 3.

A 50 mm reference standard calibration block was used as a height reference for determining of the laser propagation

Table 2 Composition of nylon reinforced samples

Sample	LDPE (%)[b]	Nylon 6 (%)[b]
4	100	0
5	80	20

[b] Gravimetric proportion

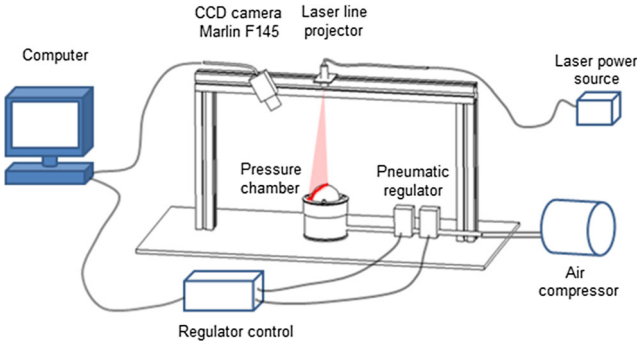

Fig. 1 Experimental setup

plane. The coefficients of the equation of the laser propagation plane (*b1*, *b2*, *b3* and *b4*) and the transformation matrix *M* were used for the transformation between image plane coordinates (u_i,v_i) and real world coordinates (X_i,Y_i,Z_i), see equation (2) [35].

$$\begin{bmatrix} X_i \\ Y_i \\ Z_i \end{bmatrix} = \begin{bmatrix} b_1 & b_2 & b_3 \\ m_{11}-u_i m_{31} & m_{12}-u_i m_{32} & m_{13}-u_i m_{33} \\ m_{21}-v_i m_{31} & m_{22}-v_i m_{32} & m_{23}-v_i m_{33} \end{bmatrix}^{-1} \begin{bmatrix} -b_4 \\ -(m_{14}-u_i m_{34}) \\ -(m_{24}-v_i m_{34}) \end{bmatrix} \tag{2}$$

Biaxial Stress–Strain Curve and Young's Modulus

Sample plates were clamped to the pressure chamber as shown in Figs. 1 and 2. Air pressure was applied to the

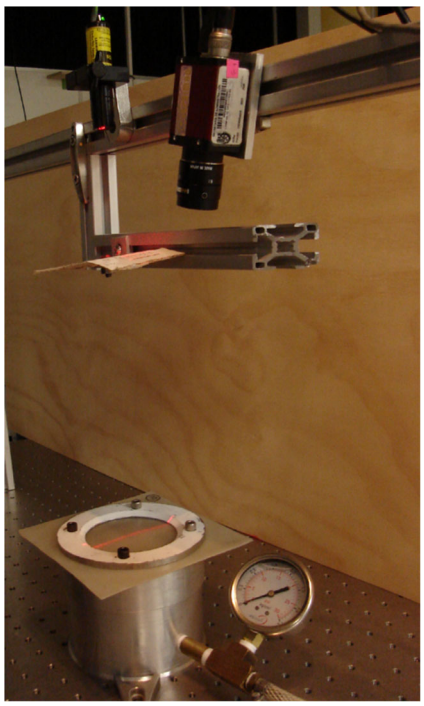

Fig. 2 Displacement measuring system

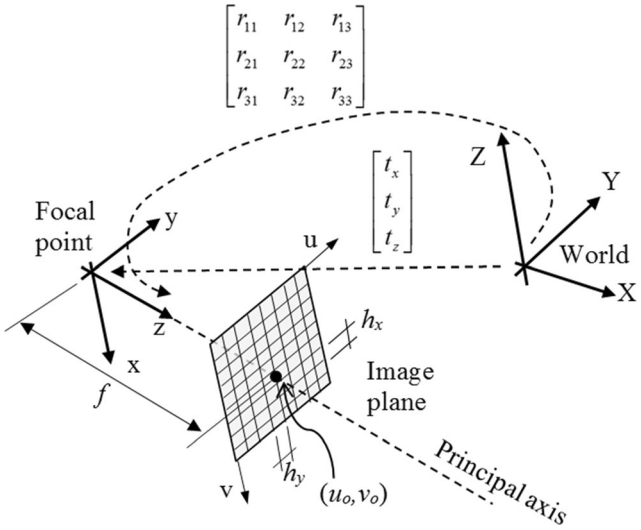

Fig. 3 Intrinsic and extrinsic parameters [37]

pressure chamber and the samples were deformed into a spherical shape. Tests were performed at room temperature, which was about 23 °C. Out-of-plane displacement h_i was measured with a laser triangulation system, see Fig. 2.

Figure 4 shows a clamped circular plate with uniform loading pressure *p*, equation (3) is widely used for calculation of biaxial stress σ_b at the point of maximum displacement '*O*', which is named the pole [7, 8, 16, 18, 22–24]. Equation (3) is known as the equation of Laplace for clamped circular plates.

$$\sigma_b = \frac{pR}{2s} \tag{3}$$

where *p* is the pneumatic pressure, *R* is the radius of curvature of the deformed sample plate, and *s* is the thickness at the pole. Considering the geometry of the deformed plate, the radius *R* is given by equation (4) [16, 29].

$$R = \frac{a^2 + h^2}{2h} \tag{4}$$

where *a* is the radius of the circular sample, *h* is the out-of-plane displacement at the pole. The thickness at the

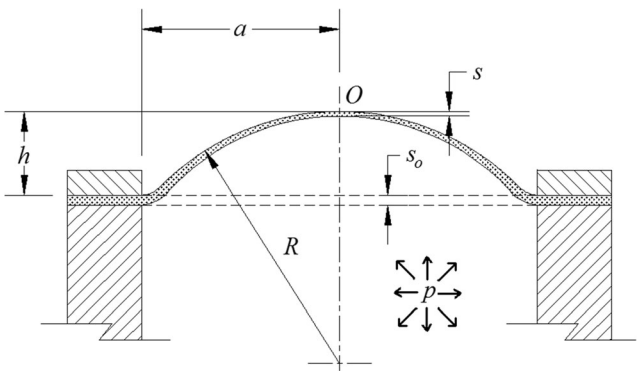

Fig. 4 Circular plate loaded with a uniform pressure *p*

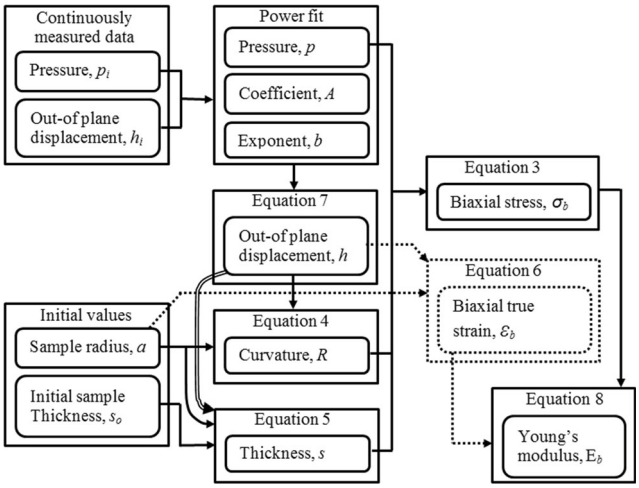

Fig. 5 Procedure for determining Young's modulus under biaxial conditions

Fig. 6 Tensile testing machine

pole decreases as the out-of-plane displacement increases. Equation (5) was used to calculate the plate thickness at the pole [16, 29].

$$s = s_0\left(1+\frac{h^2}{a^2}\right)^{-2} \tag{5}$$

where s_o is the initial thickness. The radius of the manufactured sample was 40 mm and the initial thickness was about 1.5 mm for all samples. Assuming incompressibility of the sample plate the biaxial strain at the pole was calculated with equation (6) [16, 29].

$$\varepsilon_b = \ln\left(1+\frac{h^2}{a^2}\right) \tag{6}$$

An approximation of experimental data of pressure and out-of-plane displacement at the pole is performed by a power fit. The least squares method is used for determining the coefficient A and the exponent b of the power equation, see equation (7).

$$h = Ap^b \tag{7}$$

where h is out-of-plane displacement at the pole and p is air pressure values within the range tested. From h and p are calculated biaxial stress and biaxial strain values using equation (3) thru equation (6). The determination of Young's modulus for biaxial stress condition is done by equation (8).

$$E_b = \frac{\sigma_b}{\varepsilon_b} \tag{8}$$

In Fig. 5 is presented the procedure followed for determining the biaxial stress–strain curve and Young's modulus. This procedure consisted of the following steps:

- The experimental setup in Fig. 1 was used to measure data sets of pressure p_i and out-of-plane displacement h_i.
- By least squares method, the former data sets were fitted by a power equation, see equation (7). Once known equation (7) a pressure data set p was proposed within the range tested and a data set h was calculated.
- The curvature of deformed sample plate, the data set R, was calculated using initial values of sample radius a and

Table 3 Sample dimensions values [2]

Dimension	Value (mm)
W-Width of narrow section	3.3
Wo-Width of grip section	9.4
G-Gage length	8
L-Length of reduced section	12
D-Distance between grips	25
LO-Over-all length	55
T-Thickness	1.2 - 1.6
R-Radius	13

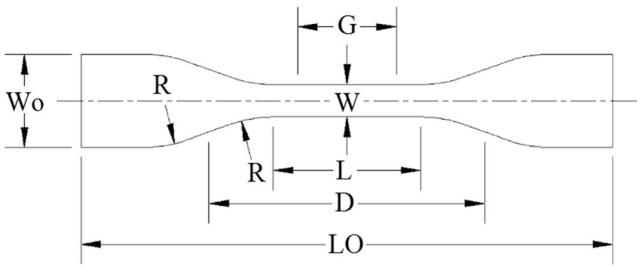

Fig. 7 Designation of sample dimensions

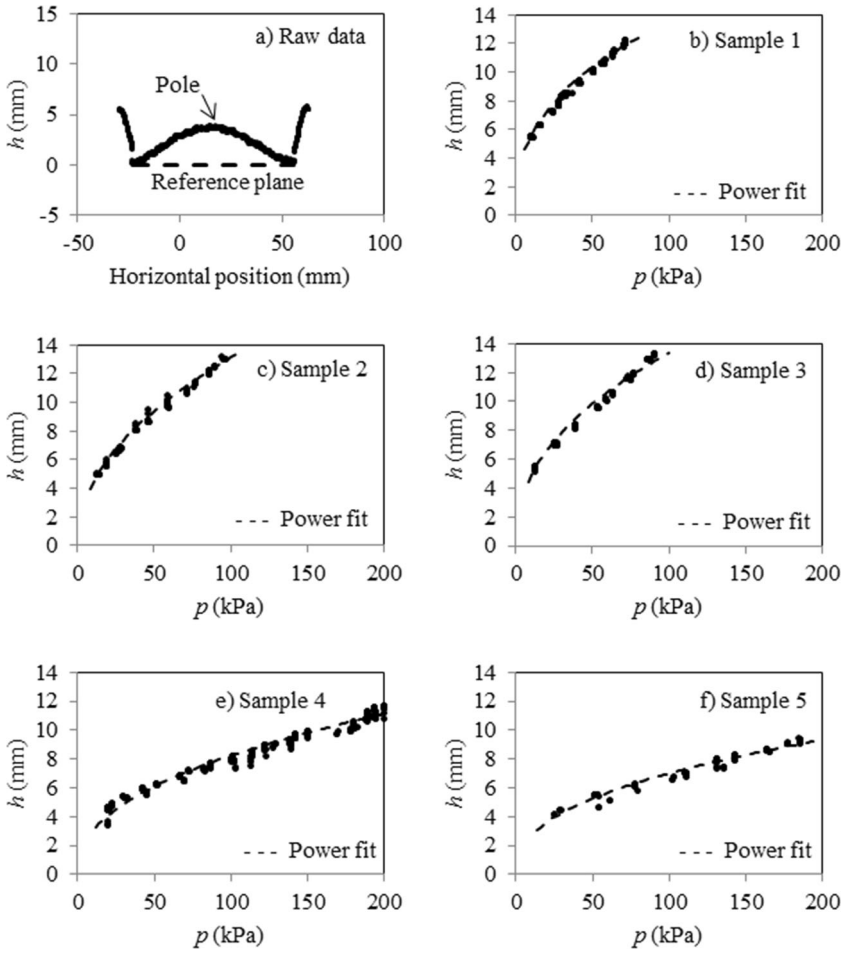

Fig. 8 Raw data and out-of-plane displacement vs. pressure

out-of-plane displacement data set h. Equation (4) was applied.

- A data set of thickness at the pole s was calculated using initial values of sample radius a, initial sample thickness s_o, and out-of-plane displacement data set h. Equation (5) was applied.
- A data set of biaxial stress σ_b was calculated from pressure data set p, curvature data set of deformed sample plate R, and data set of thickness at the pole s. Equation (3) was applied.
- A data set of biaxial strain ε_b was calculated from the out-of plane displacement data set h and the sample radius a. Equation (6) was applied.
- The Young's modulus for biaxial stress condition was calculated from the data sets of the biaxial stress σ_b, and the biaxial strain ε_b. Equation (8) was applied.

Uniaxial Test

A tensile test was performed with an INSTRON testing machine model 5565. The test was performed according to the D638-10 ASTM standard. The dimensions were according to type V specifications, obtained from die-cut, see Table 3 and Fig. 7 for dimensions of the die-cut samples. The tests were performed at a strain rate of 5 mm/min at room temperature, as seen in Fig. 6. Five coupons of sample 3 and eight coupons of all other samples were prepared and tested.

The strain was considered as the change in grip separation relative to the original grip separation. The Young's modulus was calculated dividing the stress by the corresponding strain. All Young's modulus values were computed using the average original cross sectional area at the gage length segment of the sample, referred as G in Table 3 and Fig. 7.

In the uniaxial stress–strain curves were identified toe regions which typically did not represent a property of the material. Those were deviations caused by a take-up of slack and alignment of the sample. In Fig. 9(a) the AC line defines the toe region, where C is the inflection point. The tangent at the inflection point is extended to intersect the strain axis at point B, which defines the corrected zero-strain point [2]. Using point B as zero strain, the Young's modulus at any point on the curve,

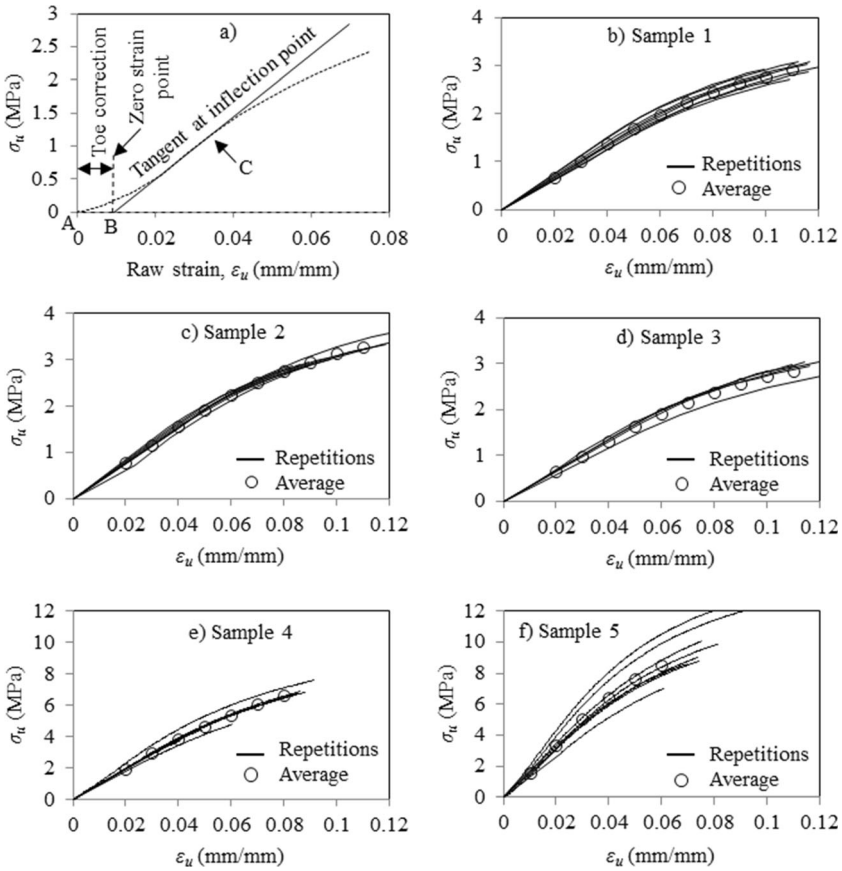

Fig. 9 Toe correction and stress–strain *curves*

was calculated as the stress divided by the strain as shown in equation (9).

$$E_u = \frac{\sigma_u}{\varepsilon_u} \tag{9}$$

Results

Biaxial Test Results

The raw data from the laser triangulation system is shown in Fig. 8(a). A second degree polynomial fit was applied to each set of raw data to get the out-of-plane displacement at the pole h_i. The sampling frequency of the out of plane displacement at the pole was 3.3 samples/s. The reference plane was established from an average position of the sample plate before air pressure application, see Fig. 8(a). A power fit is applied to get a relation between the applied pressure and the out-of-plane displacement, see Fig. 8(b) to f). The coefficients of determination, for power fit, are bigger than 0.97 for all samples.

Uniaxial Test Results

Figure 6 shows the INSTRON testing machine model 5565, it was used to test samples under uniaxial stress conditions. Five coupons of sample 3 and eight coupons of all other samples were prepared and tested. Figure 9 a) shows raw data in a graphic representation of stress versus raw strain where the elements for the toe correction are shown. Raw data is fitted by a third degree polynomial in order to identify the inflection point. The tangent at the inflection point intersects the raw strain axis at point B, this intersection defines the toe correction from point A to point B. Toe correction is calculated for each measurement repetition and subtracted from raw strain. Additionally, in Fig. 9(b) to f), five graphs of stress–strain curves after toe correction are shown. One average curve is calculated by means of a linear interpolation of each curve at discrete values of strain.

Experimental Comparison Between Uniaxial and Biaxial Tests

The behavior shown in all stress–strain curves is typical of rubber-like polymers, since no linear behavior is shown and the Young's modulus decreases as strain increases. Figure 10 shows the average curves of five tensile tests and the upper and lower limit according to the standard deviation of the uniaxial tests results. The bulge test results are presented in the same Fig. 10. Young's modulus results of sample 1 show differences from 3 to 10 MPa in the range from 0.02 up to 0.10

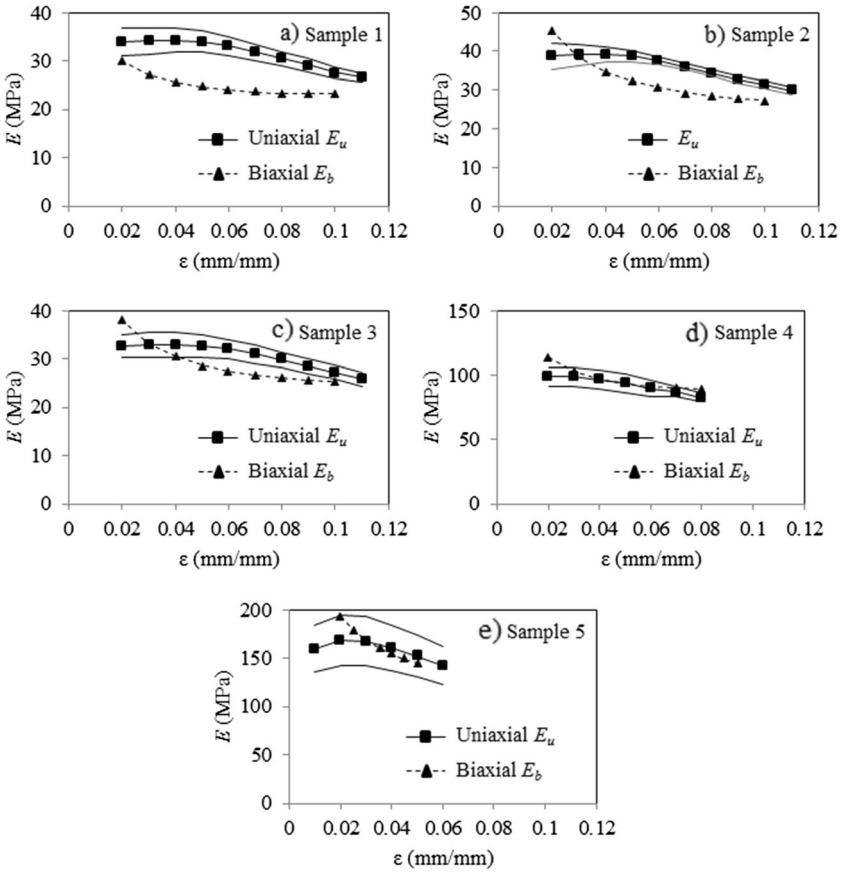

Fig. 10 Comparison of uniaxial test and biaxial test results

of strain, where biaxial test results are lower than uniaxial, see Fig. 10(a). Young's modulus results, of samples 2 and 3, show differences of 6 and 4 MPa respectively, see Fig. 10 (b) and (c). For samples 2 and 3, uniaxial Young's modulus presents steady values in the range of 0.02 to 0.04 of strain, while biaxial Young's modulus decays. Samples 4 and 5 show good agreement between uniaxial and biaxial results, since biaxial results are in between the limits defined by the standard deviation of uniaxial Young's modulus, see Fig. 10(d) and (e).

Sample 2 has the highest Young's modulus of EPDM/HDPE glass fiber reinforced blends. According to uniaxial test results, sample 1 and sample 3 have about the same stiffness since average uniaxial Young's modulus changes from 34.0 to 26.6 MPa for sample 1 and changes from 32.6 to 25.8 MPa for sample 3, see Fig. 10(a) and(c) . Uniaxial Young's modulus of sample 2 changes from 38.7 to 29.9 MPa. Biaxial test results show a different behavior for the same EPDM/HDPE glass fiber reinforced blends. Biaxial results at low strain show an increment of Young's modulus as the glass fiber content increases. Organizing from the highest glass fiber content to the lowest, sample 2 has a Young's modulus of 45.3 MPa, sample 3 has 38.1 MPa, and sample 1 has 29.9 MPa, all modulus at strain of 0.02, see Fig. 10(a), (b) and (c). As strain increases, the biaxial Young's modulus tends approximately to the same value, in spite of the glass fiber content, see Table 4.

Table 4 Young's modulus results

	Uniaxial Young's modulus		Biaxial Young's modulus	
Sample	ε_u=0.02	ε_u=0.11	ε_b=0.02	ε_b=0.10
1	34.0 MPa	26.6 MPa	29.9 MPa	23.2 MPa
2	38.7 MPa	29.9 MPa	45.3 MPa	27.4 MPa
3	32.6 MPa	25.8 MPa	38.1 MPa	25.3 MPa
	ε_u=0.02	ε_u=0.08	ε_b=0.02	ε_b=0.08
4	98.6 MPa	82.8 MPa	113.4 MPa	89.0 MPa
	ε_u=0.02	ε_u=0.06	ε_b=0.02	ε_b=0.05
5	159.6 MPa	142.4 MPa	193.5 MPa	145.3 MPa

Nylon fiber increases the Young's modulus of LDPE. Uniaxial Young's modulus changes from 98.6 to 82.8 MPa for sample 4 and changes from 159.6 to 142 MPa for sample 5, see Fig. 10(d) and (e). Biaxial Young's modulus show good agreement with uniaxial test results for strain values above 0.04. Below strain values of 0.04 biaxial Young's modulus is higher than uniaxial results, see Table 4. Nylon fiber increases the stiffness but embrittle the LDPE. The manufacturing and handling of nylon reinforced LDPE is difficult. High standard deviation of uniaxial results is a consequence of sample brittleness.

Conclusions

The stiffness of reinforced polymer blends has been investigated under uniaxial tension and biaxial stress conditions by the bulge test. Experimental results of Young's modulus have been compared and the influence of reinforcing fiber has been identified. Glass fiber increases the stiffness of EPDM/HDPE polymer blends. EPDM/HDPE samples with 0 and 2.2 % have nonsignificant differences on uniaxial Young's modulus. Biaxial Young's modulus is more sensitive to glass fiber content than uniaxial Young's modulus. Nylon fiber increases the stiffness but embrittle the LDPE. Manufacturing and handling of reinforced LDPE samples is difficult, which causes the increment of standard deviation of uniaxial Young's modulus. Uniaxial and biaxial tests have good agreement in the range tested for LDPE samples.

References

1. Sethi S, Chandra RB (2015) Environmental effects on fibre reinforced polymeric composites: evolving reasons and remarks on interfacial strength and stability. Adv Colloid Interf Sci 217:43–67. doi:10.1016/j.cis.2014.12.005
2. ASTM Standard D638–10 (2010) Standard Test Method for Tensile Properties of Plastics. ASTM International, West Conshohocken
3. ASTM Standard D882–12 (2012) Standard Test Method for Tensile Properties of Thin Plastic Sheeting. ASTM International, West Conshohocken
4. ASTM Standard guide D4762-11a (2011) Standard guide for polymer matrix composite materials. ASTM International, West Conshohocken
5. Czichos H, Saito T, Smith L (2011) Springer Handbook of Metrology and Testing. Springer, Heidelberg. doi:10.1007/978-3-642-16641-9
6. Altan T, Palaniswamy H, Bortot P, Heidl W, Bechtold A (2006) Determination of sheet material properties using biaxial bulge tests. Proc. 2nd International Conference on Accuracy in Forming Technology, Germany
7. International Standard ISO 16808:2014(E) (2014) Metallic materials – Sheet and strip – Determination of biaxial stress–strain curve by means of bulge test with optical measuring systems. Switzerland
8. Lee HS, Yoon JH, Yoo JT (2012) An experimental study on elevated temperature biaxial bulge test. Adv Mater Res 430–432:539–542. doi:10.4028/www.scientific.net/AMR.430-432.539
9. Vucetic M, Bouguecha A, Peshekhodov I, Götze T, Huinink T, Friebe H, Möller T, Behrens BA (2011) Numerical validation of analytical biaxial true stress—true strain curves from the bulge test. Intl Conf Workshop Numerical Simulation Sheet Metal Forming Process 1383:107–114. doi:10.1063/1.3623599
10. Chuanwei L, Zhanwei L, Huimin X (2014) Novel scanning electron microscope bulge test technique integrated with loading function. Rev Sci Instrum 85(10):103709. doi:10.1063/1.4897623
11. Dan W, Huimin X, Chuanwei L, Rong W (2014) Application of digital phase-shifting method in 3D deformation measurement at micro-scale by SEM. Meas Sci Technol 25(12):125002. doi:10.1088/0957-0233/25/12/125002
12. Vlassak JJ, Nix WD (1992) A new bulge test technique for the determination of Young's modulus and Poisson's ratio of thin films. J Mater Res 7(12):3242–3249. doi:10.1557/JMR.1992.3242
13. Xu D, Liehti KM (2010) Bulge testing transparent thin films with Moiré deflectometry. Exp Mech 50(2):217–225. doi:10.1007/s11340-009-9291-0
14. Çakmak UD, Kallaí I, Major Z (2014) Temperature dependent bulge test for elastomers. Mech Res Commun 60:27–32. doi:10.1016/j.mechrescom.2014.05.006
15. Çakmak UD, Major Z (2013) Experimental thermomechanical analysis of elastomers under uni- and biaxial tensile stress state. Exp Mech 53(9):653–663. doi:10.1007/s11340-013-9820-8
16. Galliot C, Luchsinger RH (2011) Uniaxial and biaxial mechanical properties of ETFE foils. Polym Test 30:356–365. doi:10.1016/j.polymertesting.2011.02.004
17. Jones A, Shaw J, Wineman A (2006) An experimental facility to measure the chemorheological response of inflated elastomeric membranes at high temperature. Exp Mech 46:579–587. doi:10.1007/s11340-006-9111-8
18. Lăzărescu L, Comșa DS, Nicodim I, Ciobanu I, Banabic D (2012) Characterization of plastic behaviour of sheet metals by hydraulic bulge test. Trans Nonferrous Met Soc Chin 22:s275–s279. doi:10.1016/S1003-6326(12)61719-1
19. Li Y, Nemes JA, Derdouri A (2000) Optical 3-D dynamic measurement system and its application to polymer membrane inflation tests. Opt Lasers Eng 33:261–276
20. Lin CS, Horng TL, Chen JH, Chen KH, Wu JJ, Chen CY, Ma SH (2014) Mechanical properties measurement of polymer films by bulge test and fringe projection. Adv Mater Sci Eng ID170279. doi:10.1155/2014/170279
21. Machado G, Favier D, Chagnon G (2011) Membrane curvatures and stress–strain full fields of axisymmetric bulge tests from 3D-DIC measurements. Theory and validation on virtual and experimental results. Exp Mech 52(7):865–880. doi:10.1007/s11340-011-9571-3
22. Mott PH, Roland CM, Hassan SE (2003) Strains in an inflated rubber sheet. Rubber Chem Technol 76(2):326–333. doi:10.5254/1.3547746
23. Reuge N, Schmidt FM, Le Maoult Y, Rachik M, Abbé F (2001) Elastomer biaxial characterization using bubble inflation technique. Polym Eng Sci 41(3):522–531. doi:10.1002/pen.10749
24. Sasso M, Palmieri G, Chiappini G, Amodio D (2008) Characterization of hyperelastic rubber-like materials by biaxial and uniaxial stretching test based on optical methods. Polym Test 27(8):995–1004. doi:10.1016/j.polymertesting.2008.09.001
25. Shaw JA, Jones AS, Wineman AS (2005) Chemorheological response of elastomers at elevated temperatures: experiments and simulations. J Mech Phys Solids 53(12):2758–2793. doi:10.1016/j.jmps.2005.07.004
26. Treloar LRG (1944) Strains in an inflated rubber sheet and the mechanism of bursting. Rubber Chem Technol 17(4):957–967. doi:10.5254/1.3546716
27. Wineman A, Shaw J (2005) Influence of thermally induced chemorheological changes on the inflation of spherical elastomeric membranes. J Elast 80:73–95. doi:10.1007/s10659-005-9020-6
28. Zitzumbo R, Ornelas-Rodriguez FJ, Lopez M, Alonso S, Yanez J, Avalos F, Ortiz JC, Zizumbo A (2006) Laser technology application: deformation and elastic recovery of semi- crystalline polymers. Eur Polym J 42:1298–1304. doi:10.1016/j.eurpolymj.2005.12.016
29. Charalambides M, Wanigasooriya L, Williams G, Chakrabarti S (2002) Biaxial deformation of dough using the bubble inflation technique. I. Experimental. Rheol Acta 41(6):532–540. doi:10.1007/s00397-002-0242-2

30. Moraes C, Simmons C, Sun Y (2013) System, apparatus and method for applying mechanical force to a material. United States patent 8557582 B2
31. Dong C (2012) A regression model for analysing the non-linearity of laser triangulation probes. Int J Adv Manuf Technol 59:691–695. doi:10.1007/s00170-011-3517-x
32. Vukašinovic N, Bracun D, Mozina J (2012) A new method for defining the measurement-uncertainty model of CNC laser-triangulation scanner. Int J Adv Manuf Technol 58:1097–1104. doi:10.1007/s00170-011-3467-3
33. Bouguet JY (2013) Camera calibration toolbox for Matlab. http://www.vision.caltech.edu/bouguetj/calib_doc/index.html. Accessed 07 February 2014
34. Zhang Z (1999) Flexible camera calibration by viewing a plane from unknown orientations. Proc IEEE Intl Conf Comput Vis 1: 666–673. doi:10.1109/ICCV.1999.791289
35. Horaud R, Monga O (1995) Vision par ordinateur: outils fondamentaux. Deuxième edition. Editions Hermès. 425
36. Gorthi SS, Rastogi P (2010) Fringe projection techniques: whither we are? Opt Lasers Eng 48:133–140. doi:10.1016/j.optlaseng.2009.09.001
37. Cyganek B, Siebert JP (2009) An introduction to 3D computer vision techniques and algorithms. John Wiley & Sons. ISBN: 978-0-470-01704-3